

**PdAg/CNT Catalyzed Alcohol Oxidation Reaction for High-Performance  
Anion Exchange Membrane Direct Alcohol Fuel Cell (Alcohol = Methanol,  
Ethanol, Ethylene Glycol and Glycerol)**

Ji Qi<sup>†</sup>, Neeva Benipal<sup>†</sup>, Changhai Liang<sup>‡</sup>, Wenzhen Li<sup>†\*</sup>

<sup>†</sup>Department of Chemical and Biological Engineering, Iowa State University, Ames, Iowa  
50011, United States

<sup>‡</sup>School of Chemical Engineering, Dalian University of Technology, Dalian, Liaoning 116023,  
China.

---

\*Corresponding author: Tel: +15152944582, *E-mail address*: wzli@iastate.edu

## ABSTRACTS

PdAg supported on carbon nanotubes (PdAg/CNT) with an average particle size of 2.7 nm is prepared by an aqueous phase reduction method for alcohol oxidation reaction in direct alcohol fuel cells. In a half-cell system with three electrodes, the peak mass activity of PdAg/CNT reaches  $0.105 \text{ mA } \mu\text{g}_{\text{Pd}}^{-1}$ ,  $0.305 \text{ mA } \mu\text{g}_{\text{Pd}}^{-1}$ ,  $2.105 \text{ mA } \mu\text{g}_{\text{Pd}}^{-1}$ , and  $8.53 \text{ mA } \mu\text{g}_{\text{Pd}}^{-1}$  for methanol oxidation reaction, ethanol oxidation reaction, ethylene glycol oxidation reaction, and glycerol oxidation reaction, respectively, in 1 M KOH 0.1 M alcohol electrolyte. These values are higher than the mass activity of Pd/CNT at the same applied potential. With PdAg/CNT ( $0.5 \text{ mg}_{\text{Pd}} \text{ per MEA}^{-1}$ ) as an anode catalyst, a direct methanol fuel cell, a direct ethanol fuel cell, a direct ethylene glycol fuel cell and a direct glycerol fuel cell achieve peak power densities of  $135.1 \text{ mW cm}^{-2}$ ,  $202.3 \text{ mW cm}^{-2}$ ,  $245.2 \text{ mW cm}^{-2}$ , and  $276.2 \text{ mW cm}^{-2}$ , with corresponding peak mass activities of  $270.2 \text{ mW mg}_{\text{Pd}} \text{ per MEA}^{-1}$ ,  $404.6 \text{ mW mg}_{\text{Pd}} \text{ per MEA}^{-1}$ ,  $490.4 \text{ mW mg}_{\text{Pd}} \text{ per MEA}^{-1}$ , and  $552.4 \text{ mW mg}_{\text{Pd}} \text{ per MEA}^{-1}$ , respectively, at 80 °C and ambient pressure. Ag has shown excellent activity towards aldehyde (formaldehyde, acetaldehyde, and glyoxylate) oxidation, thus, the enhancement in alcohol oxidation on PdAg/CNT is proposed due to Ag's promotion of intermediate aldehyde oxidation. PdAg/CNT also improves the fuel efficiency of glycerol oxidation by contributing to the C-C bond cleavage of  $\text{C}_3$  glycerol to  $\text{C}_2$  oxalate.

## 1. Introduction

People are forced to replace limited fossil fuels with renewable and clean energy sources to alleviate the environmental pollution and global climate change. [1] The easy handling and large volumetric energy density of alcohol make direct alcohol fuel cells (DAFCs) a potential solution to the current energy issues. [2] Anion exchange membrane DAFCs (AEM-DAFCs) are attracting increasing research efforts as a result of the fast kinetics of anode alcohol oxidation reaction (AOR) and cathode oxygen reduction reaction (ORR) in alkaline media. [3] Although non-precious iron-based catalysts [4-6] or carbon based metal-free catalysts [7, 8] can be used for ORR at the cathode side in anion exchange membrane fuel cells (AEMFCs), high loading precious metal is still required for AOR at the anode side in low-temperature AEM-DAFCs. As a result, the cost of catalyst layer accounts for more than 50 % of the total cost of AEM-DAFCs[9], constituting a major technical obstacle hindering the commercialization of AEM-DAFCs. To overcome this issue, there is an urgent need to develop catalysts with large electrochemically active surface area (ECSA), high mass activity, and intrinsic activity.

Platinum-based catalysts are the most widely used type in low-temperature DAFCs (< 100 °C). [9, 10] Although Pt's catalytic activity with respect to methanol oxidation reaction (MOR) [11], ethanol oxidation reaction (EOR) [12], ethylene glycol oxidation (EGOR) [13]

and glycerol oxidation reaction (GOR) [14] can be very high in DAFCs, its scarcity results in a high price ( $> \$50 \text{ g}^{-1}$ ). One method of reducing the cost of catalyst layer is to lower down the loading of Pt, while another method is to replace Pt with more abundant and less expensive Pd. To prepare highly active Pd-based catalysts, a number of strategies have been investigated, including controlling the morphology of Pd [15-19], alloying other elements to prepare Pd-M catalyst [20-25], and improving the surface area of the catalyst support [26-28]. However, since Pd based catalysts' activity and the ability to cleave C-C bonds for long chain alcohol have to be further improved, there is an urgent need not only to increase the mass activity but also to increase the intrinsic activity of Pd-based precious metal anode catalysts.

In the electrochemical AOR process, carbonyl groups are detected on the surface of electrodes by infrared spectroscopy (IR)[29-32] while carboxylic groups are detected in the liquid electrolyte containing reaction products by high-performance liquid chromatography (HPLC) [5, 33, 34]. The aldehyde is considered to be either an intermediate or a reaction product of electrocatalytic AOR. [35-40] Thus, we proposed that a faster reaction rate of electrocatalytic aldehyde oxidation reaction (ADOR) can contribute to the acceleration of AOR, leading to a higher electricity output in DAFCs. In study of electrocatalytic ADOR, previous researchers have successfully used bulk metal anodes [41], Au nanoparticles[42], and Pd nanoparticles supported on carbon nanotubes (Pd/CNT) [43] for formaldehyde ( $\text{C}_1$  aldehyde) oxidation reaction. However, because  $\text{C}_{2+}$  alcohols have other  $\text{C}_{2+}$  aldehydes as

AOR reaction intermediates, activities of different supported nanoparticles with respect to various aldehydes must still be compared to discover an active site facilitating AOR by accelerating ADOR for high-performance DAFCs fed with fuels such as methanol, ethanol, ethylene glycol and glycerol.

In this study, alloyed PdAg nanoparticles supported on carbon nanotubes (PdAg/CNT) were prepared for AOR with an aqueous-phase reduction method excluding the usage of surfactant, which offered several advantages. First, Ag/CNT electrochemically catalyzes the ADOR more efficiently than Pt/CNT, Pd/CNT, and Au/CNT. Pd is a well-known electrocatalyst for AOR, but not the best one for ADOR. Although it exhibits little activity towards AOR in alkaline media, Ag can help Pd in accelerating the reaction rate of ADOR. Thereby we propose the AOR enhancement is due to Ag facilitating ADOR, thus facilitating the whole AOR network. Second, by alloying Pd with Ag, the particle size of Ag can be greatly reduced from 17.7 nm (Ag/CNT) to 2.7 nm (PdAg/CNT) without covering the catalyst's surface with surfactants, leading to a high ECSA for both Pd and Ag components. Third, PdAg/CNT can also cleave the C-C bond of long-chain polyol such as glycerol, providing a high fuel efficiency. Fourth, the carbon nanotube (CNT) support with high electrical conductivity, remarkable mechanical strength, and good thermal stabilities [44] will form three dimensional (3D) electrode structure on the membrane electrode assembly (MEA) and enhance the mass transport of alcohol and OH<sup>-</sup>, resulting in an even higher catalyst

utilization ratio in actual fuel cell operation. In a three electrode half-cell system, the peak mass activity of PdAg/CNT reaches  $0.105 \text{ mA } \mu\text{g}_{\text{Pd}}^{-1}$ ,  $0.305 \text{ mA } \mu\text{g}_{\text{Pd}}^{-1}$ ,  $2.105 \text{ mA } \mu\text{g}_{\text{Pd}}^{-1}$ , and  $8.53 \text{ mA } \mu\text{g}_{\text{Pd}}^{-1}$  for MOR, EOR, EGOR and GOR in 1 M KOH 0.1 M alcohol electrolyte, respectively. With PdAg/CNT ( $0.5 \text{ mg}_{\text{Pd per MEA}}^{-1}$ ) as the anode catalyst, the AEM-DAFC can achieve peak power densities (PPD) of  $135.1 \text{ mW cm}^{-2}$ ,  $202.3 \text{ mW cm}^{-2}$ ,  $245.2 \text{ mW cm}^{-2}$  and  $276.2 \text{ mW cm}^{-2}$ , with corresponding peak mass activities of  $270.2 \text{ mW mg}_{\text{Pd per MEA}}^{-1}$ ,  $404.6 \text{ mW mg}_{\text{Pd per MEA}}^{-1}$ ,  $490.4 \text{ mW mg}_{\text{Pd per MEA}}^{-1}$  and  $552.4 \text{ mW mg}_{\text{Pd per MEA}}^{-1}$  at  $80 \text{ }^\circ\text{C}$  and ambient pressure, when using methanol, ethanol, ethylene glycol and glycerol, respectively, as fuel.

## 2. Experimental

### 2.1. Chemicals:

The short multi-walled CNT (10-20 nm outer diameter, 0.5-2  $\mu\text{m}$  length) was purchased from Cheaptubes Inc.  $\text{H}_2\text{PtCl}_6 \cdot x\text{H}_2\text{O}$  (~38% Pt basis),  $\text{Pd}(\text{NO}_3)_2 \cdot 2\text{H}_2\text{O}$  (~40% Pd basis),  $\text{AuCl}_3$  (99%),  $\text{AgNO}_3$  (99%), potassium sulfate (99%), polytetrafluoroethylene water solution (60%), potassium hydroxide (85%), 1-propanol (99.5%), methanol (99.8%), ethanol (99.5%), ethylene glycol (99.8%) and glycerol (99.5%) were bought from Sigma-Aldrich Co. The catalyst 4020 was ordered from Acta, Inc. Sodium borohydride (99%) and sodium citrate dihydrate (99%) were manufactured by Acros Organics. All the chemicals were used as

received without further purification.

## 2.2. Preparation and physical characterization of different catalysts with X-ray diffraction (XRD) and transmission electron microscopy (TEM)

All the monometallic and bimetallic catalysts including Pt/CNT, Pd/CNT, Au/CNT, Ag/CNT, PdAg/CNT, and PdAg<sub>3</sub>/CNT (20 % metal loading) were prepared using an aqueous-phase reduction method. In a typical preparation process of Pt/CNT for example, the catalyst precursor was first dissolved in citric acid water solution. Then the reducing agent solution was prepared by ultrasonically dissolving sodium borohydride into a citric acid water solution. The precursor solution was quickly poured into the reducing agent solution under vigorous stirring, leading to a hydrosol solution of nanoparticles. Both catalyst precursor and sodium borohydride reducing agent were stabilized by citric acid so that the reducing process was controlled at an appropriate rate which ensures that the size of the nanoparticles is small enough for a large surface area. If the citric acid were not added, the sodium borohydride would decompose to hydrogen so the catalyst precursor would not be fully reduced. Short CNTs functionalized by carboxylate acid groups were sonicated in water for 15 min with shaking. The CNTs water mixture was added into the hydrosol solution immediately after the reduction of the precursor, followed by 12 h of dropwise addition of potassium sulfate solution into the mixture to facilitate the deposition of nanoparticles. The carboxylic acid

groups make CNTs more hydrophilic leading to improved dispersion in water. Therefore, the as-prepared nanoparticles hydrosol will make a better contact with the CNT supports during deposition. After being filtrated and dried overnight in a vacuum oven at room temperature, Pt/CNT catalyst with a loading of 20 wt% was obtained.

The structure and morphology of all the catalysts were characterized by X-ray diffraction (XRD), and transmission electron microscopy (TEM). A Scintag XDS-2000  $\theta/\theta$  diffractometer employed to collect the XRD patterns produces Cu K $\alpha$  radiation ( $\lambda = 1.5406 \text{ \AA}$ ) operated under a 35 mA filament current and a 45 kV tube voltage with a continuous scan rate of 1.2 degree per minute. Due to its relative isolation, the (220) peak was selected for calculating the mean crystallite sizes of all the catalysts based on the Debye-Scherrer formula:

$$L = \frac{0.9\lambda_{K\alpha}}{B_{2\theta} \cos \theta_{\max}} \quad (1)$$

where L is the mean crystallite size,  $\lambda$  is the wavelength of the x-ray (1.5406 $\text{\AA}$ ), B is the full width at half-maximum of the peak (rad) and  $\theta_{\max}$  is the Bragg angle (rad) of the (220) peak.

The transmission electron microscopy (TEM) images were collected on JEOL JEM-4000FX with an accelerating voltage of 200 kV.

2.3. Electrocatalytic activities of different catalysts with respect to alcohol and aldehyde oxidation in a three electrode half-cell system



A three-electrode, water-jacket-integrated glass cell (AFCELL3, Pine Instrument) including a glassy carbon working electrode (AFE3T050GC, Pine Instrument), a Hg/HgO reference electrode (MMO, CHI152, CH Instruments), and a platinum wire counter electrode (AFCTR1, Pine Instrument) was employed to perform cyclic voltammetry (CV) tests. After being shaken in an ultrasonic ice-water bath for 2 min, 2.5 mg catalyst in 4.0 mL 1-propanol and 1.0 mL DI water formed a uniform black colored catalyst ink with a concentration of 0.5 mg mL<sup>-1</sup>. The DI water improved dispersion of CNT supports with hydrophilic carboxylic acid groups. The catalyst ink was added dropwise onto the surface of the glassy carbon electrode (GCE) with a glass syringe. For monometallic catalyst, the weight of metal on the GCE was 1 µg. For the PdAg bimetallic catalyst, the weight of Pd on the GCE was 1 µg since silver is relatively cheap and inactive with respect to alcohol oxidation within the fuel cell anode potential. 1.0 M potassium hydroxide (KOH) and 0.1 M aldehyde or alcohol was used as the electrolyte for the CV tests. With a scan rate of 50 mV s<sup>-1</sup>, the CV tests were conducted at room temperature in a nitrogen atmosphere.

Typical core criteria for catalysts evaluation includes activity, selectivity, durability, and reaction conditions, among which turnover frequency (TOF) is the most important parameter reflecting a catalyst's intrinsic activity. TOF<sub>e<sup>-</sup></sub> is defined with respect to transferred electrons as instead of converted substrates as follows:

$$TOF_{e^-} = \frac{I}{F \times ECSA \times m \times SAD}$$

where  $I$  is the current in the external circuit;  $F$  is the Faraday constant; ECSA is the electrochemically active surface area;  $m$  is the mass of metal catalyst on the electrode; SAD is the surface atomic density of difference facets (Supplementary information, Table S7).

$$ECSA = \frac{Q_{ox}}{m \times q_{coulombic}}$$

where  $Q_{ox}$  is the integrated charge of the metal oxide reduction peak,  $m$  is the mass of the metal catalyst deposited onto the electrode, and  $q$  is the coulombic charge of different reduction peaks corresponding to the scan range. The ECSA of Pt/CNT[45], Pd/CNT[46], Au/CNT[47] and Ag/CNT[48] was calculated corresponding to coulombic charge of 0.420 mC cm<sup>-2</sup>, 0.385 mC cm<sup>-2</sup>, 0.245 mC cm<sup>-2</sup> and 0.400 mC cm<sup>-2</sup>, respectively. (Supplementary information, Figure S1) To evaluate the specific activity, the ECSA of Pd in the Pd-based bimetallic catalyst was calculated by intergrating the reduction peak of palladium oxidation.

#### 2.4. Direct alcohol fuel cells with Pd-based anode catalysts

The fuel cell test stand (850e Scribner-Associates) was operated in scan current mode to collect polarization curves within a 0 to 5 A current range. The experiments were performed under ambient pressure and at various temperatures without setting any vertex current. The fuel cell temperature was controlled by a feedback loop composed of electric heating rods and a thermocouple-based thermometer in the stainless steel end plates. The anode catalyst ink (10 mg<sub>catalyst</sub> cm<sup>-3</sup> concentration) was prepared by mixing catalyst and polytetrafluoroethylene (PTFE) (95:5 mass ratio) in iso-propanol solvent by ultra-sonication

in an ice-water bath for 10 min with shaking. The cathode catalyst ink containing 30 wt% of ionomer (AS4 Tokuyama) as binder and anion conductor was prepared similarly to the anode catalyst ink using 1-propanol as solvent. The Pd loading on the anode catalyst-coated carbon cloth was controlled to be  $0.5 \text{ mg cm}^{-2}$  by alternately weighing and spraying the anode catalyst ink onto the carbon cloth substrate. The cathode catalyst-coated anion exchange membrane was fabricated by airbrushing  $3 \text{ mg cm}^{-2}$  of the cathode catalyst (4020 Acta) onto an anion exchange membrane (A901 Tokuyama). The  $5 \text{ cm}^2$  membrane electrode assembly (MEA) was prepared by combining standalone anode (catalysts coated carbon cloth) and an integrated cathode with an anion exchange membrane (catalysts coated anion exchange membrane with carbon paper as backing layer). The MEA was placed between two serpentine graphite flow field plates that were further pressed from both sides by two gilded plate current collectors. The default testing conditions[14] were anode fuel: 6.0 M KOH, 3.0 M alcohol,  $4.0 \text{ ml min}^{-1}$ ; cathode fuel:  $200 \text{ ml min}^{-1} \text{ O}_2$ , ambient pressure; temperature (anode fuel/cathode fuel/cell): 25/80/80 °C or 25/60/60 °C.

## 2.5 Product analysis of GOR in AEM-DGFC with PdAg/CNT anode catalyst

23.5 ml of 1.0 M glycerol + 6.0 M KOH solution was cycled between a plastic vessel and the anode chamber via a closed loop by a peristaltic pump ( $1.0 \text{ min}^{-1}$  flow rate), while the high-purity  $\text{O}_2$  (>99.999%) was fed into the cathode compartment at a flow rate of  $100 \text{ sccm min}^{-1}$  under ambient pressure. The electrocatalytic GOR was conducted by

controlling the fuel cell voltage of 0.2 V. Samples were analyzed by an HPLC using an Alltech, OA-1000 column equipped with a refractive index detector (RID, Agilent G1362A) and a variable wavelength detector (VWD, 220 nm, Agilent G1314A). 5 mM of aqueous sulfuric acid eluent at a flow rate of 0.3 ml min<sup>-1</sup> was applied to the product separation. 20 μl of the diluted sample (10 times) was injected into the HPLC system. Products were identified and quantified by comparison with authentic samples.

The product selectivity, glycerol conversion, and fuel efficiency were calculated by the following equations:

$$S = \frac{\text{moles of } C_2 \text{ or } C_3 \text{ product}}{\text{total moles of } C_2 \text{ and } C_3 \text{ products}} \times 100\% \quad (1)$$

$$X_g = \left(1 - \frac{\text{residual moles of glycerol after reaction}}{\text{total moles of glycerol}}\right) \times 100\% \quad (2)$$

$$\begin{aligned} \varepsilon_f &= \varepsilon_e \times X_g = \frac{n_{\text{actual}}}{n_{\text{completely oxidized}}} \times X_g = \frac{Q}{n_{\text{completely oxidized}} mF} \times X_g \\ &= \frac{\int_{t_1}^{t_2} I dt}{n_{\text{completely oxidized}} mF} \times X_g \end{aligned} \quad (3)$$

where S is the selectivity of one C<sub>2</sub> or C<sub>3</sub> product; X<sub>g</sub> is the conversion of glycerol; ε<sub>f</sub> is the fuel efficiency; ε<sub>e</sub> is the electron efficiency; *n<sub>actual</sub>* is the average number of electrons transferred from a single glycerol molecule in the electrochemical GOR; *n<sub>completely oxidized</sub>* (=14) is number of the electrons extracted from single glycerol molecule when it is completely oxidized; *Q* is the actual charge integrated from the *I-t* curve (Figure 7); *m* is the molar amount of glycerol consumed in the electrocatalytic GOR; *t*<sub>1</sub> and *t*<sub>2</sub> are the reaction time bounds for integration; *I* is instantaneous cell current; *F* is Faraday's constant.

## 2.6. Supplementary calculations for explanations of Ag's high activity with respect to aldehyde oxidation

All the orbital energy calculations were performed with the Gaussian 09 program package. [49] Orbital energy levels and the isosurfaces of the frontier orbitals of aldehydes containing C, H, and O atoms (atomic coordinates listed in Supplementary information, Table S1-Table S5) were computed at Modified Neglect of Diatomic Overlap (MNDO) [50] level of theory to properly fit the experimental data of ionization energy and electron affinity. Different methods (Austin Model 1 (AM1) method[51] and Parameterized Model number 3 (PM3) method [52]) were used to calculate the chemical hardness to check reproducibility and accuracy by comparing the calculations with experimental results (Supplementary information, Table S6).

## 3. Results and discussion

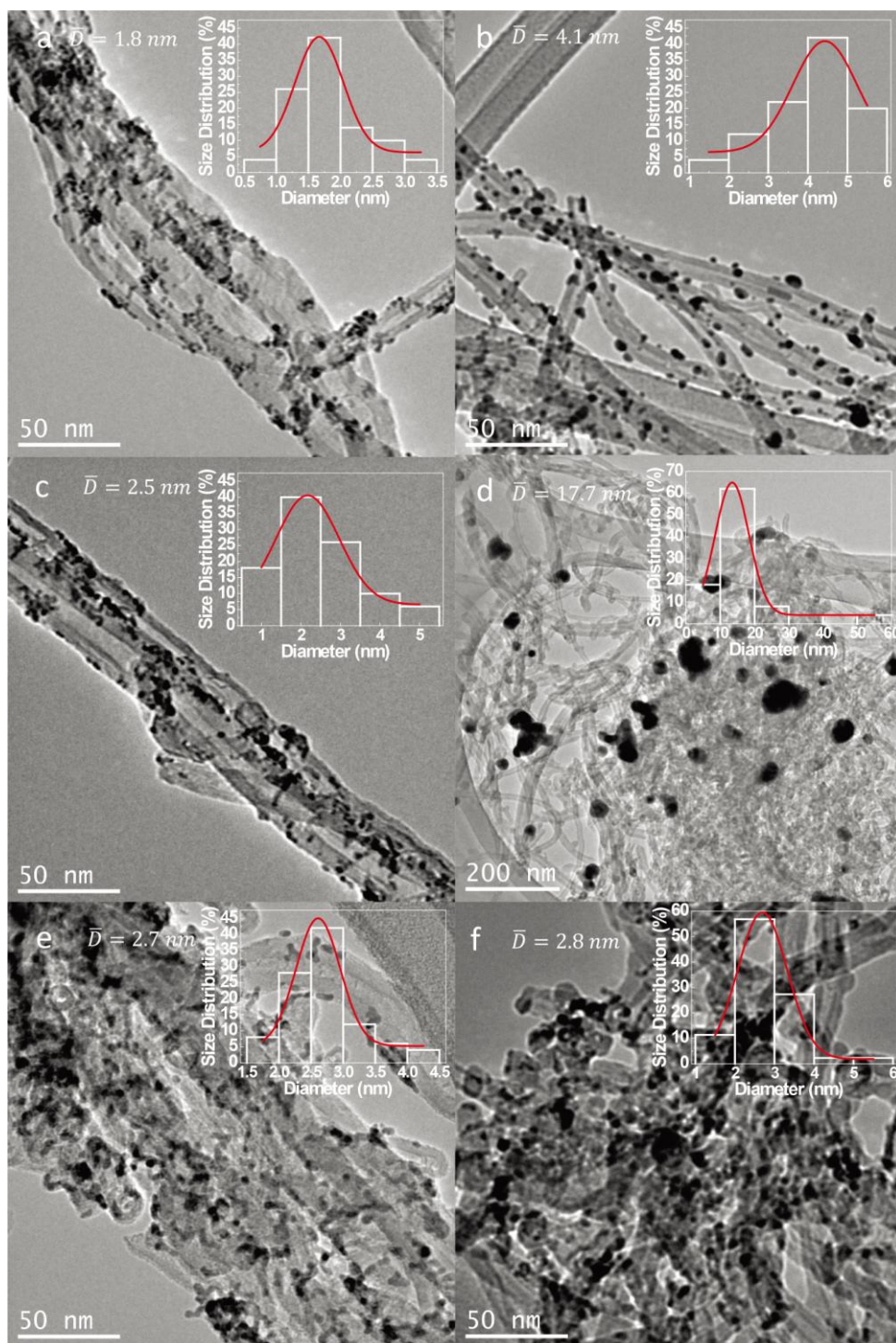


**Figure 1.** Bright field transmission electron microscopy (TEM) images and corresponding particle size histograms of (a) Pt/CNT, (b) Au/CNT, (c) Pd/CNT, (d) Ag/CNT, (e) PdAg/CNT and (f) PdAg<sub>3</sub>/CNT.

Figure 1 shows the TEM images of carbon nanotubes (CNT) supported Pt, Au, Pd, and Ag nanoparticle catalysts. The average particle sizes of Pt/CNT, Au/CNT, Pd/CNT,

Ag/CNT, PdAg/CNT, and PdAg<sub>3</sub>/CNT measured by randomly counting 100 particles are 1.8 nm, 4.1 nm, 2.5 nm, 17.7 nm, 2.7 nm, and 2.8 nm, respectively. The particle sizes of supported Pd nanoparticles prepared by electroless procedures usually range from 3 nm to 25 nm[3]. The aqueous phase reduction method prepared Pd/CNT, PdAg/CNT, and PdAg<sub>3</sub>/CNT have well-distributed Pd-based nanoparticles with an average measured particle size less than 3 nm.

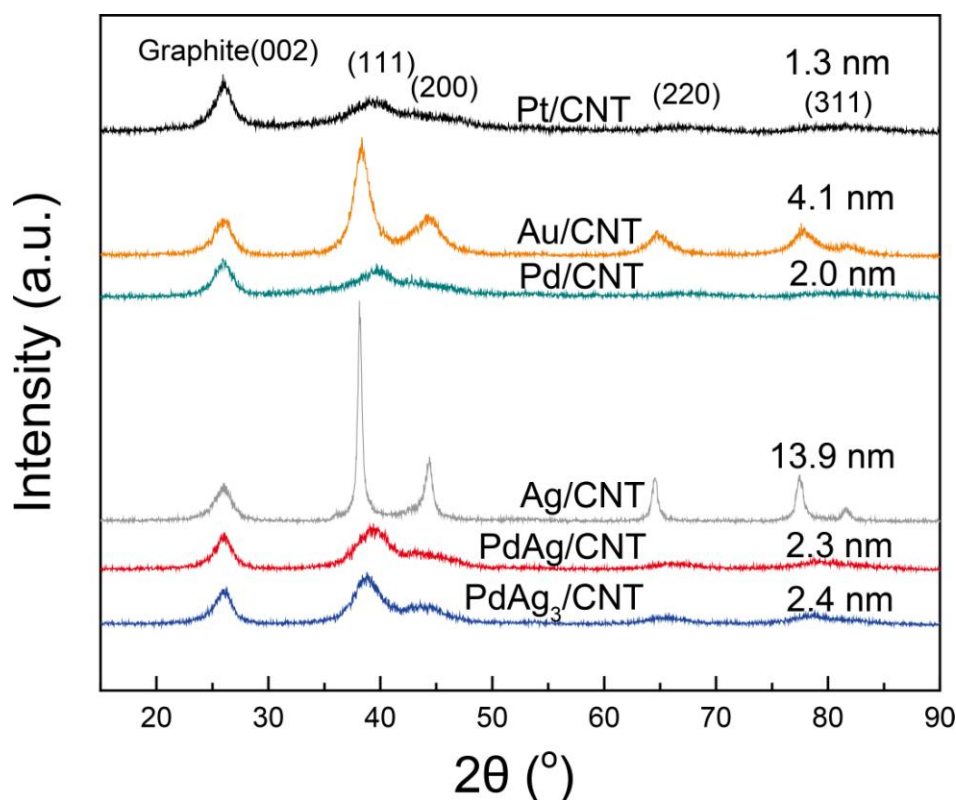


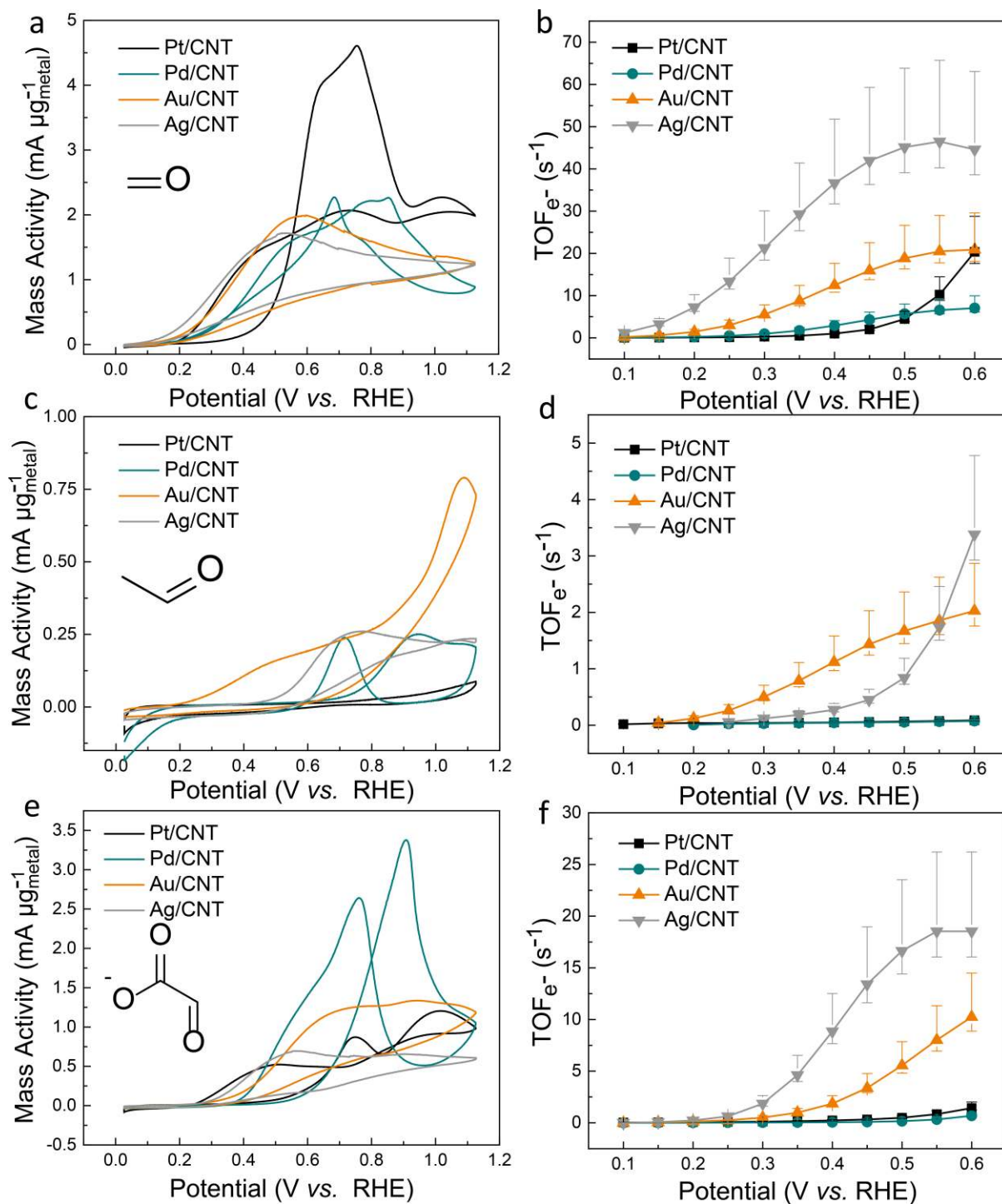
**Figure 2.** XRD patterns of Pt/CNT, Au/CNT, Pd/CNT, Ag/CNT, PdAg/CNT, and PdAg<sub>3</sub>/CNT (20% total metal loading) with their particle sizes calculated from (220) diffraction peak.

The XRD patterns of Pt/CNT, Au/CNT, Pd/CNT, Ag/CNT, PdAg/CNT, and PdAg<sub>3</sub>/CNT are depicted in Figure 2, with peak positions of (1 0 0), (2 0 0), (2 2 0), and (3 1 1) facets marked. The face-centered cubic (FCC) structured Pt/CNT, Au/CNT, Pd/CNT,

Ag/CNT, PdAg/CNT and PdAg<sub>3</sub>/CNT have mean crystallite size of 1.3 nm, 4.1 nm, 2.0 nm, 13.9 nm, 2.3 nm and 2.4 nm, calculated using the full width half maximum (FWHM) method at the Gaussian-fitted (220) peaks using Scherrer's equation. Earlier researchers successfully prepared Pd/C [53], Pd-S-HCNF [54], Pd/CNT [55], Pd@WC-Mo<sub>2</sub>C/C [56], PdSb<sub>0.15</sub>/C [21], PdNi/C [57], PdAg/C[58], and PdAu/C [59] for AOR with mean crystallite sizes of 4.0 nm, 5.1 nm, 10.5 nm, 6.1 nm, 3.8 nm, 3.1 nm, 3.7 nm and 3.7 nm, respectively. The mean crystallite sizes of Pd/CNT and PdAg/CNT are further reduced to 2.0 nm and 2.3 nm in the current work by the aqueous phase reduction method without using surfactants. The average mean crystallite size determined by XRD is consistent with but smaller than the average particle size measured by TEM images. This phenomenon was also observed for Pt-based[14, 60], Pd-based [23], and Au-based[61] catalysts, which can be attributed to several possible reasons. First, particles smaller than 0.5 nm are hard to be recognized in TEM images but can be reflected by calculation based on XRD patterns. Second, XRD peak broadening is caused not only by crystallite size but also by factors such as dislocations, stacking faults, twinning, micro stresses, grain boundaries, sub-boundaries, coherency strain, and chemical heterogeneities[62]. Third, the mean crystallite size obtained from XRD patterns represents the single crystal size while the average particle size measured from TEM images includes the agglomeration effect of single crystal particles as a result of intermolecular forces. [58] No obvious phase separation is observed for PdAg/CNT and PdAg<sub>3</sub>/CNT since alloyed PdAg



peaks are between Pd peaks and Ag peaks.

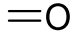
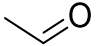
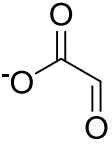


**Figure 3.** Cyclic voltammograms and corresponding  $\text{TOF}_{e^-}$  range in low temperature direct alcohol fuel cell anode potential window ( $< 0.7$  V vs. RHE) of Pt/CNT, Pd/CNT, Au/CNT and Ag/CNT for aldehyde oxidation in  $\text{N}_2$  purged 1.0 M KOH + 0.1 M formaldehyde (a and b), acetaldehyde (c and d), and glyoxylate (e and f) at 50  $\text{mV s}^{-1}$ , room temperature.

The mass activity and TOF of Pt/CNT, Pd/CNT, Au/CNT and Ag/CNT with respect to electrocatalytic aldehyde oxidation obtained from cyclic voltammograms are compared (Figure 3 and Table 1). Formaldehyde, acetaldehyde, and glyoxylate are selected as aldehyde substrate because the aldehyde group is easier to be oxidized than the substituent connected to it. This ensures that the current generated can properly evaluate the catalysts' activity for ADOR in the potential range not high enough to oxidize the catalysts. Detailed discussion of substrate selection is summarized in the supplementary information. The mass activity and onset potential are two indicators of apparent activity in cyclic voltammetry, while the former is affected by the particle size of catalysts to a larger extent. The highest peak values of mass activity in the forward scan of cyclic voltammograms (Figure 3) for formaldehyde oxidation, acetaldehyde oxidation, and glyoxylate oxidation on Pt/CNT ( $4.6 \text{ mA } \mu\text{g}^{-1}$  at  $0.78 \text{ V}$ ), Au/CNT ( $0.8 \text{ mA } \mu\text{g}^{-1}$  at  $1.06 \text{ V}$ ) and Pd/CNT ( $3.3 \text{ mA } \mu\text{g}^{-1}$  at  $0.88 \text{ V}$ ) are positioned at least  $400 \text{ mV}$  more positive than their corresponding onset potentials (Pt/CNT:  $0.33 \text{ V}$ ; Au/CNT:  $0.19 \text{ V}$ ; Pd/CNT:  $0.44 \text{ V}$ ), and are out of the fuel cell anode potential range (from onset potential to  $< 0.7 \text{ V}$  vs. RHE). Taking into account the particle size and potential window mismatch factors, the onset potential rather than (peak) mass activity is employed as the major indicator of apparent activity. Accordingly, due to  $> 100 \text{ mV}$  more negative onset potential (Table 1), Ag/CNT, and Au/CNT are more active than Pd/CNT or Pt/CNT towards aldehyde oxidation. When it comes to intrinsic activity, TOF has been defined as the molar

ratio of converted original substrate and exposed active sites in unit time[63, 64]. Herein, to evaluate electrocatalysts' effectiveness towards series reactions or reaction networks including the original substrate and all the reaction intermediates, the  $TOF_{e^-}$  was defined as the number of electrons extracted from the original reactant or reaction intermediates by each exposed active site in unit time.

**Table 1.** Apparent and intrinsic activities comparison of different monometallic catalysts

Entry	Catalyst	Substrate name and molecular structure	Onset Potential (V vs RHE)	Mass Activity at 0.6 V vs RHE ( $\text{mA } \mu\text{g}^{-1}_{\text{metal}}$ )	Specific Activity at 0.6 V vs RHE ( $\text{mA cm}^{-2}_{\text{metal}}$ )	Turnover Frequency Range for Polycrystalline catalysts at 0.6 V vs RHE( $\text{s}^{-1}$ ) <sup>a</sup>		
						Minimum	Medium	Maximum
1	Pt/CNT		0.326	3.085	4.242	17.622	20.348	28.777
2	Pd/CNT	Formaldehyde	0.186	1.703	1.493	6.103	7.048	9.967
3	Au/CNT		0.086	1.990	4.060	18.100	20.900	29.558
4	Ag/CNT		0.026	1.640	8.543	44.619	44.593	63.064
5	Pt/CNT		0.726	0.013	0.018	0.074	0.086	0.121
6	Pd/CNT	Acetaldehyde	0.596	0.018	0.016	0.064	0.074	0.105
7	Au/CNT		0.186	0.193	0.394	1.756	2.028	2.868
8	Ag/CNT		0.376	0.124	0.647	2.926	3.379	4.778
9	Pt/CNT	Glyoxylate	0.426	0.216	0.297	1.236	1.427	2.018
10	Pd/CNT		0.436	0.165	0.145	0.593	0.685	0.968
11	Au/CNT		0.296	0.976	1.991	8.877	10.250	14.496
12	Ag/CNT		0.226	0.682	3.551	16.052	18.535	26.212

<sup>a</sup>To evaluate the range of  $TOF_{e^-}$  for polycrystalline catalysts, it is assumed that the polycrystalline surface can be approximately treated as a linear combination of the major facets. For fcc structure, the minimum, medium and maximum  $TOF_{e^-}$  can be calculated with surface atomic density of (111), (100), (110) surfaces, respectively.

The  $TOF_{e^-}$  of polycrystalline FCC-structured Pt/CNT, Pd/CNT, Au/CNT and Ag/CNT is within the range calculated based on (111), (100), and (110) as their major facets (Figure 3 and Table 1). At 0.6 V anode potential, the  $TOF_{e^-}$  of Ag for ADOR is 1.7–2.2 times, 6.3–45.7 times and 2.2–39.5 times that of Au, Pd, and Pt, respectively. The activity sequence of different catalysts toward ADOR is Ag/CNT>Au/CNT>>Pd/CNT and Pt/CNT within the anode potential of fuel cell. We also attempted to explain Ag's high activity towards ADOR using the descriptor of orbital energy difference matching from the energy balance point of view in the charge transfer process from molecular level. (Supplementary information)

However, since the mean crystallite size of Ag (13.9 nm) measured by XRD is 10.7, 7.0 and 3.7 times that of Pt (1.3 nm), Pd (2.0 nm), and Au (3.8 nm) respectively, its electrochemically active surface area (Supplementary information, Table S7) and mass activity are relatively low. Pd has high activity and stability toward alcohol oxidation[3], especially in the hydroxyl group deprotonation process, and its particle size is one order of magnitude smaller than Ag. So to take advantage of the high  $TOF_{e^-}$  of aldehyde oxidation on Ag in the ADOR process, the particle size of Ag is controlled by alloying with Pd so that the catalyst's surface is clean without being covered by capping agents.

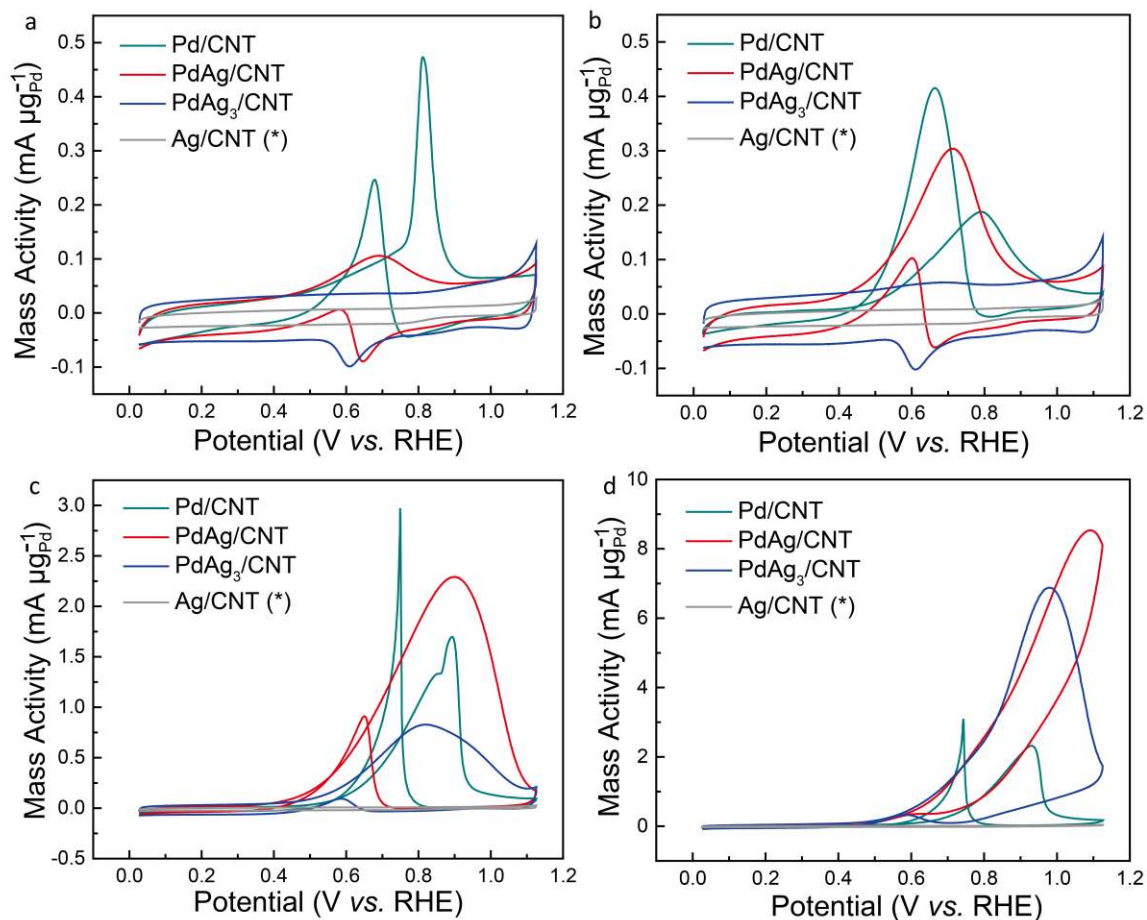


**Figure 4.** Cyclic voltammograms of Pd/CNT, PdAg/CNT, PdAg<sub>3</sub>/CNT and Ag/CNT for alcohol oxidation in N<sub>2</sub> purged 1.0 M KOH + 0.1 M (a) methanol, (b) ethanol, (c) ethylene glycol, (d) glycerol at 50 mV s<sup>-1</sup>, room temperature. (\*) Unlike mass activity of Pd/CNT, PdAg/CNT, and PdAg<sub>3</sub>/CNT, mass activity of Ag/CNT (mA μg<sub>Ag</sub><sup>-1</sup>) is calculated based on the mass of Ag instead of mass of Pd since there's no Pd on the electrode.

Based on the cyclic voltammograms performed in 1 M KOH 0.1 M alcohol electrolyte (Figure 4), the peak mass activity of PdAg/CNT for MOR (0.105 mA μg<sub>Pd</sub><sup>-1</sup>), EOR (0.305 mA μg<sub>Pd</sub><sup>-1</sup>), EGOR (2.105 mA μg<sub>Pd</sub><sup>-1</sup>) and GOR (8.53 mA μg<sub>Pd</sub><sup>-1</sup>) are higher than the mass activity of Pd/CNT and PdAg<sub>3</sub>/CNT at the same applied potential. Moreover, the specific activity of PdAg/CNT for EGOR, EOR, and GOR (Supplementary information, Figure S2) is higher than that of Pd/CNT within the fuel cell anode potential (< 0.6 V vs. RHE). However, the specific activity of PdAg<sub>3</sub>/CNT for alcohol oxidation reaction is lower

than that of PdAg/CNT, indicating the further addition of Ag will lower down the specific activity of Pd. Alloying Pd and Ag reduces the particle size of Ag to less than 3 nm without use of surfactants (Figure 1, Supplementary information, Table S7), raising the catalyst's activity towards alcohol oxidation reaction network (Figure 4, and Supplementary information, Figure S2) likely by exploiting spillover of aldehyde intermediates to Ag active sites with high  $\text{TOF}_e^-$  toward aldehyde oxidation. In the electrocatalytic oxidation process of alcohol, some desorbed reaction products are hard to be re-adsorbed and get further oxidized[34]. Altering the active sites by spillover effects before the active reaction intermediates leave the catalyst layer can therefore achieve the deep oxidation of the alcohol. Furthermore, Ag exhibits no obvious activity towards methanol, ethanol, and ethylene glycol oxidation reactions within the whole potential window (Supplementary information, Figure S3), while it shows very slight activity with respect to glycerol oxidation reaction when the potential is higher than 1.0 V vs RHE. In general, it can be concluded that Ag is relatively catalytically inactive towards alcohol oxidation within the fuel cell anode potential window (<0.6 V vs RHE). The relative inertness of Ag towards alcohol oxidation suggests that a catalyst is necessary for extracting electrons from the initial deprotonation of a hydroxy group in alkaline media, which is not only a consequence of interactions between hydroxide anions, acidic hydroxyl hydrogen and a conductive electrode surface. As a result, an excessive amount of Ag in a bimetallic catalyst will deteriorate initial deprotonation of

hydroxyl groups by diluting and blocking Pd active sites, as depicted in Figure 4 and Figure

S2.

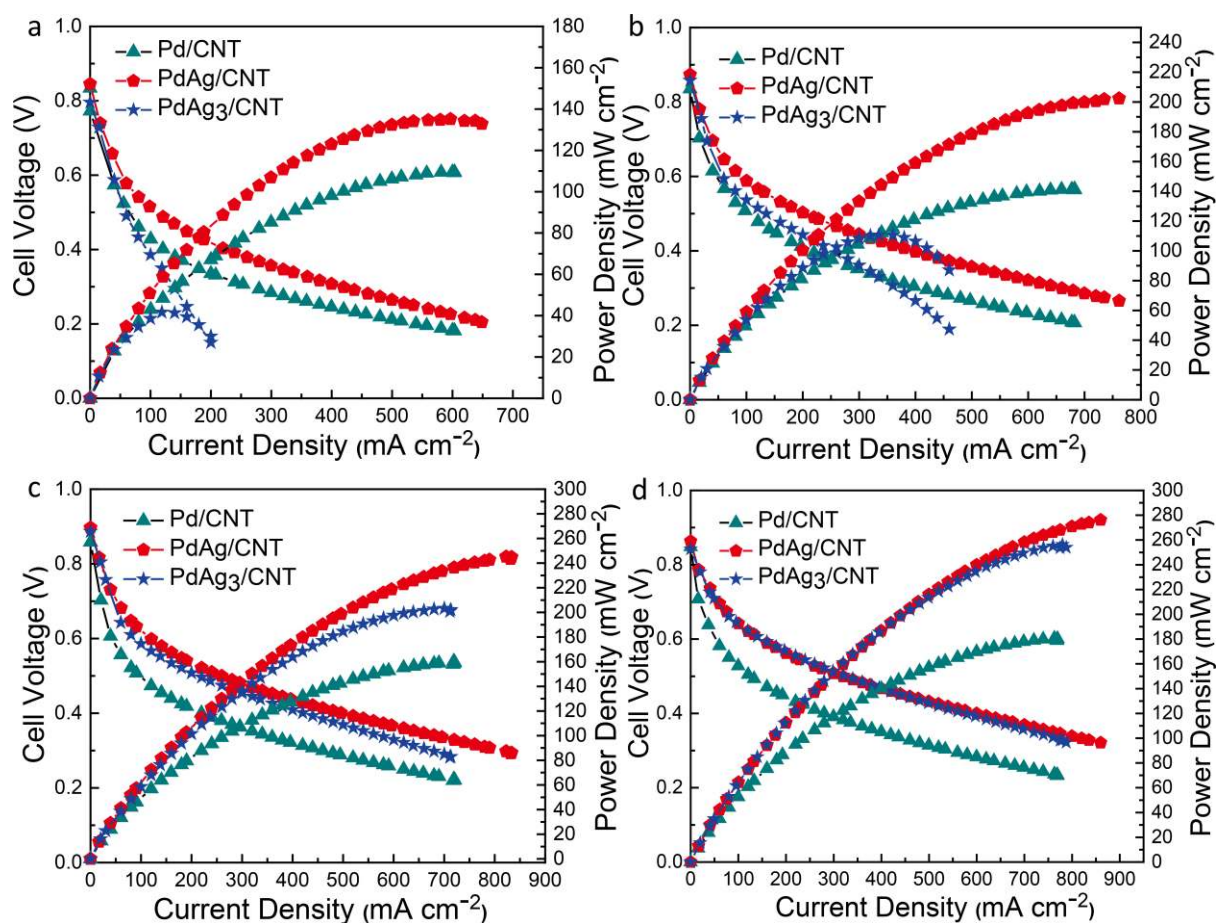


**Figure 5.** Polarization and power density curves of direct alcohol AEMFCs with different anode catalysts ( $\text{Pd/CNT}$ ,  $\text{PdAg/CNT}$  and  $\text{PdAg}_3/\text{CNT}$ ,  $0.5 \text{ mg}_{\text{Pd}} \text{ cm}^{-2}$ ) at optimized operating conditions. AEM: Tokuyama A901; cathode catalyst: Fe-based catalyst (Acta 4020),  $3.0 \text{ mg}_{\text{catalyst}} \text{ cm}^{-2}$ ; anode fuel: 6.0 M KOH + 3.0 M (a) methanol, (b) ethanol, (c) ethylene glycol and (d) glycerol,  $4.0 \text{ ml min}^{-1}$ ; cathode fuel: 200 sccm  $\text{O}_2$ , ambient pressure; temperature (anode fuel/cathode fuel/cell): 25/80/80 °C.

To further confirm Ag-catalyzed aldehyde oxidation can facilitate alcohol oxidation, we tested the single direct alcohol fuel cells with  $\text{PdAg/CNT}$  anode catalyst. As shown in Figure 5, low-temperature anion exchange membrane fuel cells (AEMFCs) fueled with methanol, ethanol, ethylene glycol and glycerol have peak power densities of  $135.1 \text{ mW cm}^{-2}$ ,  $202.3 \text{ mW cm}^{-2}$ ,  $245.2 \text{ mW cm}^{-2}$ , and  $276.2 \text{ mW cm}^{-2}$ , which are 23.3 %, 43.2 %, 53.1 % and

53.0 % higher than that of AEMFCs with Pd/CNT as anode catalyst respectively. By diluting and blocking Pd active sites, an increase in the Ag atomic ratio will suppress the hydroxyl group deprotonation process and accelerate the aldehyde oxidation process, which are more effective on Pd and Ag, respectively. Influenced by this tradeoff, the total electron release rate of these two processes has a relationship with the Ag atomic ratio (Supplementary information, Figure S4). It is noteworthy that the more hydroxyl groups in an alcohol molecule, the larger contribution of Ag facilitated aldehyde oxidation to the total discharge performance will be, owing to the existence of more possible aldehyde intermediates. The performance of AEMFC (Figure 5 and Supplementary information, Figure S5) with the PdAg<sub>3</sub>/CNT anode catalyst will consequently be closer to that of AEMFCs with the PdAg/CNT anode catalyst when the hydroxyl group number per molecule in the substrate increases from 1 (methanol and ethanol) to 2 (ethylene glycol) and to 3 (glycerol).



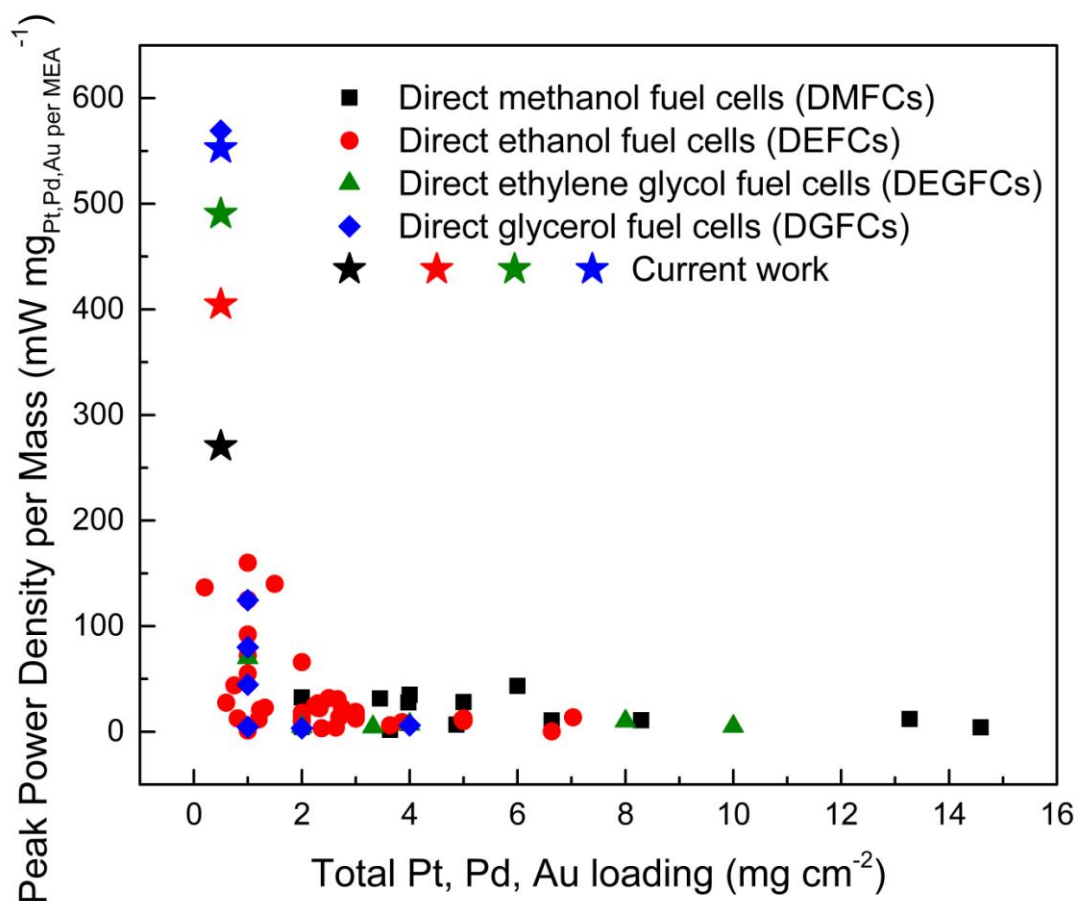


**Figure 6.** State-of-the-art performances of low temperature ( $< 100\text{ }^{\circ}\text{C}$ ) oxygen or air based DAFCs fed with methanol, ethanol, ethylene glycol and glycerol. Peak power density per mass (Pt, Pd, Au) versus total Pt, Pd, Au loading in the MEA is exhibited for the major DAFCs systems including direct methanol fuel cells (DMFCs) [65-76], direct ethanol fuel cells (DEFCs) [1, 12, 77-118], direct ethylene glycol fuel cells (DEGFCs) [13, 68, 119-122], and direct glycerol fuel cells (DGFCs) [5, 14, 68, 101, 123-125].

Figure 6 summarizes the state-of-the-art performances of low temperature ( $< 100\text{ }^{\circ}\text{C}$ ) oxygen or air based DAFCs fed with methanol, ethanol, ethylene glycol, and glycerol. In the current work, the PPDs per mass catalyst reach  $270.2\text{ mW mg}_{\text{Pd per MEA}}^{-1}$ ,  $404.6\text{ mW mg}_{\text{Pd per MEA}}^{-1}$ ,  $490.4\text{ mW mg}_{\text{Pd per MEA}}^{-1}$  and  $552.4\text{ mW mg}_{\text{Pd per MEA}}^{-1}$  for DMFC, DEFC, DEGFC, and DGFC, which are among the highest published results. Although the peak mass activity of DGFC ( $552.4\text{ mW mg}_{\text{Pd per MEA}}^{-1}$ ) with PdAg/CNT anode catalyst is slightly lower than that

(569.2 mW mg<sub>Pt</sub> per MEA<sup>-1</sup>) of DGFC with surface dealloyed PtCo supported on carbon nanotube (SD-PtCo/CNT) anode catalyst, PdAg/CNT is still a generally cost-effective replacement of Pt in DAFCs.

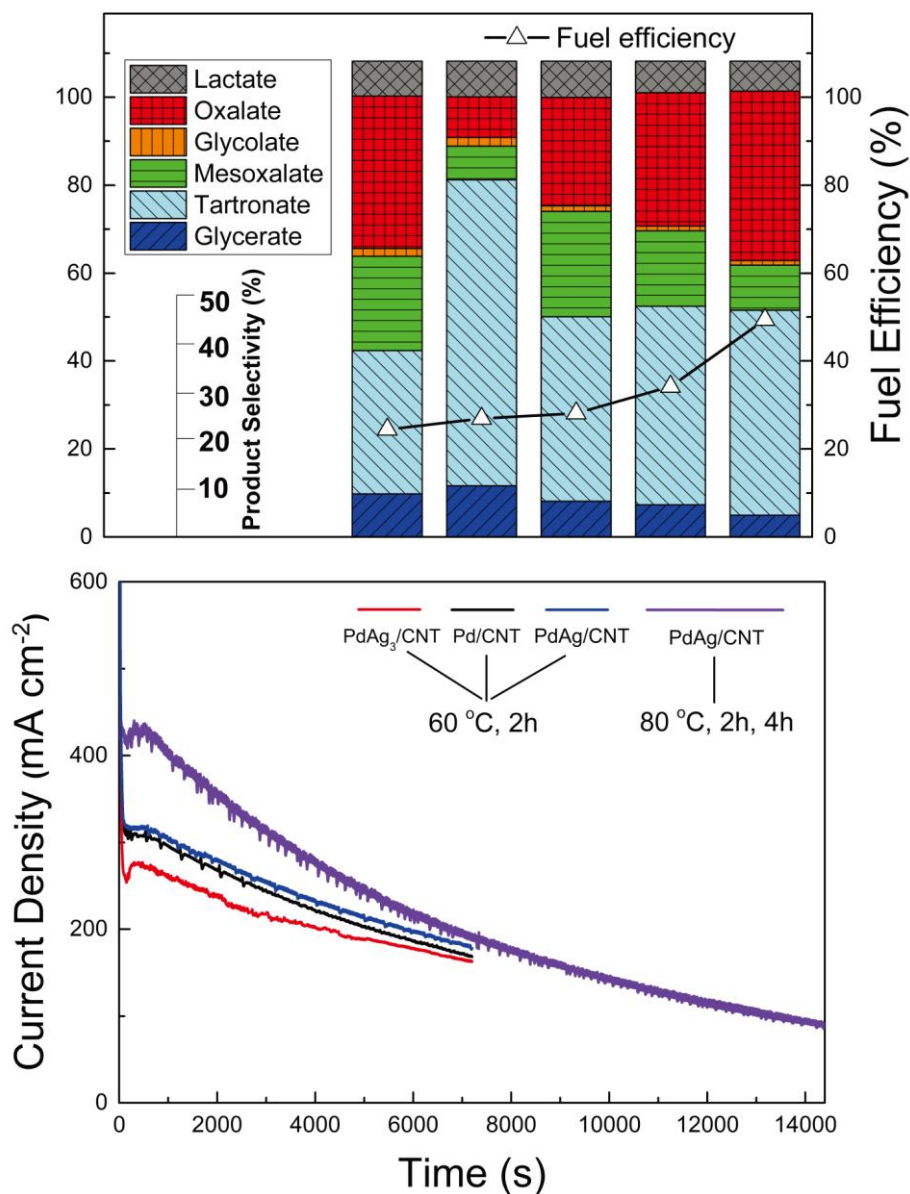


**Figure 7.** Electrocatalytic selective oxidation of glycerol on Pd/CNT, PdAg/CNT, and PdAg<sub>3</sub>/CNT in DGFC for C-C bond cleavage and fuel efficiency analysis. Anode catalyst: Pd/CNT, PdAg/CNT or PdAg<sub>3</sub>/CNT (0.5 mg<sub>Pd</sub> cm<sup>-2</sup>); Cathode catalyst: Fe-Cu-based catalyst (Acta 4020, 3 mg cm<sup>-2</sup>), anion exchange membrane (A901, Tokuyama Inc.). Anode fuel: 6.0 M KOH + 1.0 M glycerol, 23.5 ml, 1.0 ml min<sup>-1</sup>; Cathode fuel: high purity O<sub>2</sub>, 100 ml min<sup>-1</sup>, ambient pressure.; Cell voltage: 0.2 V; Cell temperature: 60 °C or 80 °C reaction time: 2 h or 4 h.

We further examined the alcohol oxidation products on PdAg/CNT anode catalyst in single fuel cell setting. Figure 7 shows C-C bond cleavage and fuel efficiency analysis of glycerol (long chain C<sub>3</sub> polyol) oxidation on Pd/CNT, PdAg/CNT, and PdAg<sub>3</sub>/CNT in DGFC. For 2 h of electrocatalytic GOR in DGFC at 60 °C, the selectivity of C<sub>2</sub> oxalate on Pd/CNT, PdAg/CNT and PdAg<sub>3</sub>/CNT is 8.6 %, 22.8 %, and 32.0 % while the corresponding conversion of glycerol is 55.3 %, 49.3 %, and 46.6 %, respectively, indicating that the addition of silver can contribute to the C-C bond cleavage of C<sub>3</sub> glycerol to C<sub>2</sub> oxalate and lowers glycerol conversion. Balancing the tradeoff between the selectivity of C<sub>2</sub> oxalate and conversion of glycerol, a DGFC with the PdAg/CNT anode catalyst generates the highest current density and fuel efficiency during the electrocatalytic GOR. The fuel efficiency on PdAg/CNT is 28.1 %, which is 4.5 % and 15.2 % higher than that on Pd/CNT and PdAg<sub>3</sub>/CNT. After 4 h of GOR at 80 °C on the PdAg/CNT anode catalyst, the selectivity of C<sub>2</sub> oxalate, conversion of glycerol and fuel efficiency of GOR further increases to 85.8% and 49.3 %, making PdAg/CNT not only a highly active but also a highly efficient catalyst for GOR and DGFC in alkaline media.

#### **4. Conclusion**

In summary, PdAg/CNT was prepared for AOR in AEM-DAFCs via an aqueous-phase reduction method excluding the usage of surfactant. With PdAg/CNT (0.5

$\text{mg}_{\text{Pd per MEA}}^{-1}$ ) as the anode catalyst, the AEM-DAFCs achieve PPD of  $135.1 \text{ mW cm}^{-2}$ ,  $202.3 \text{ mW cm}^{-2}$ ,  $245.2 \text{ mW cm}^{-2}$ , and  $276.2 \text{ mW cm}^{-2}$ , with corresponding peak mass activities of  $270.2 \text{ mW mg}_{\text{Pd per MEA}}^{-1}$ ,  $404.6 \text{ mW mg}_{\text{Pd per MEA}}^{-1}$ ,  $490.4 \text{ mW mg}_{\text{Pd per MEA}}^{-1}$ , and  $552.4 \text{ mW mg}_{\text{Pd per MEA}}^{-1}$  at  $80 \text{ }^\circ\text{C}$  and ambient pressure, when using methanol, ethanol, ethylene glycol, and glycerol, respectively, as fuel. The high activity of PdAg/CNT towards AOR in AEM-DAFCs can be attributed to several reasons. First, Ag/CNT electrochemically catalyzes the ADOR more efficiently than Pt/CNT, Pd/CNT, and Au/CNT. Although not active towards AOR in alkaline media, we proposed Ag can help Pd to accelerate the reaction rate of ADOR and thereby the whole AOR network. Second, by alloying Pd with Ag, the particle size of Ag can be greatly reduced from  $17.7 \text{ nm}$  (Ag/CNT) to  $2.7 \text{ nm}$  (PdAg/CNT) without covering the catalyst's surface by surfactants, leading to a high ECSA for both Pd and Ag components. Third, PdAg/CNT can cleave the C-C bond of long chain polyols such as glycerol, providing a high fuel efficiency. Fourth, CNT support with high electrical conductivity, remarkable mechanical and thermal stabilities will form 3D electrode structure on MEA and enhance the mass transport of alcohol and  $\text{OH}^-$ , resulting in an even higher catalyst utilization ratio in actual fuel cell operation.

## **Acknowledgements**

We gratefully acknowledge the US National Science Foundation (CBET-1159448 and

CBET-1501124) for funding. J. Qi thanks the financial support from the Chinese Scholarship Council.

## References

- [1] Y. Chen, M. Bellini, M. Bevilacqua, P. Fornasiero, A. Lavacchi, H.A. Miller, L. Wang, F. Vizza, *ChemSusChem*, 8 (2015) 524-533.
- [2] J. Zhang, S. Lu, Y. Xiang, P.K. Shen, J. Liu, S.P. Jiang, *ChemSusChem*, 8 (2015) 2956-2966.
- [3] C. Bianchini, P.K. Shen, *Chemical Reviews*, 109 (2009) 4183-4206.
- [4] L. An, T.S. Zhao, L. Zeng, X.H. Yan, *International Journal of Hydrogen Energy*, 39 (2014) 2320-2324.
- [5] X. Han, D.J. Chadderdon, J. Qi, L. Xin, W. Li, W. Zhou, *International Journal of Hydrogen Energy*, 39 (2014) 19767-19779.
- [6] Y. Li, Y. He, *RSC Advances*, 4 (2014) 16879-16884.
- [7] J. Qi, N. Benipal, D.J. Chadderdon, J. Huo, Y. Jiang, Y. Qiu, X. Han, Y.H. Hu, B.H. Shanks, W. Li, *Carbon*, 89 (2015) 142-147.
- [8] J. Qi, N. Benipal, H. Wang, D.J. Chadderdon, Y. Jiang, W. Wei, Y.H. Hu, W. Li, *ChemSusChem*, 8 (2015) 1147-1150.
- [9] L. An, T.S. Zhao, Y.S. Li, *Renewable & Sustainable Energy Reviews*, 50 (2015) 1462-1468.
- [10] P. Joghee, J.N. Malik, S. Pylypenko, R. O'Hayre, *MRS Energy & Sustainability - A Review Journal*, 2 (2015) null-null.
- [11] D. Hwan Jung, C. Hyeong Lee, C. Soo Kim, D. Ryul Shin, *Journal of Power Sources*, 71 (1998) 169-173.
- [12] Q. Wang, G.Q. Sun, L. Cao, L.H. Jiang, G.X. Wang, S.L. Wang, S.H. Yang, Q. Xin, *Journal of Power Sources*, 177 (2008) 142-147.
- [13] V. Livshits, E. Peled, *Journal of Power Sources*, 161 (2006) 1187-1191.
- [14] J. Qi, L. Xin, Z. Zhang, K. Sun, H. He, F. Wang, D. Chadderdon, Y. Qiu, C. Liang, W. Li, *Green Chemistry*, 15 (2013) 1133-1137.
- [15] S. Dash, N. Munichandraiah, *Journal of the Electrochemical Society*, 160 (2013) H197-H202.
- [16] A.-L. Wang, H. Xu, J.-X. Feng, L.-X. Ding, Y.-X. Tong, G.-R. Li, *Journal of the American Chemical Society*, 135 (2013) 10703-10709.
- [17] A.A. Daryakenari, D. Hosseini, T. Saito, A. Apostoluk, C.R. Muller, J.-J. Delaunay, *RSC Advances*, 5 (2015) 52578-52587.

- [18] O.O. Fashedemi, H.A. Miller, A. Marchionni, F. Vizza, K.I. Ozoemena, *Journal of Materials Chemistry A: Materials for Energy and Sustainability*, 3 (2015) 7145-7156.
- [19] Y. Zhang, Q. Huang, G. Chang, Z. Zhang, T. Xia, H. Shu, Y. He, *Journal of Power Sources*, 280 (2015) 422-429.
- [20] Z. Zhang, C. Zhang, J. Sun, T. Kou, C. Zhao, *RSC Advances*, 2 (2012) 11820-11828.
- [21] J. Cai, Y. Huang, Y. Guo, *International Journal of Hydrogen Energy*, 39 (2014) 18256-18263.
- [22] L. Li, M. Chen, G. Huang, N. Yang, L. Zhang, H. Wang, Y. Liu, W. Wang, J. Gao, *Journal of Power Sources*, 263 (2014) 13-21.
- [23] E.J. Lim, Y. Kim, S.M. Choi, S. Lee, Y. Noh, W.B. Kim, *Journal of Materials Chemistry A: Materials for Energy and Sustainability*, 3 (2015) 5491-5500.
- [24] H. Rostami, A.A. Rostami, A. Omrani, *International Journal of Hydrogen Energy*, 40 (2015) 10596-10604.
- [25] L. Zhang, H. Wang, X. Li, F. Xia, Y. Liu, X. Xu, J. Gao, F. Xing, *Electrochimica Acta*, 172 (2015) 42-51.
- [26] J. Zhao, M. Shao, D. Yan, S. Zhang, Z. Lu, Z. Li, X. Cao, B. Wang, M. Wei, D.G. Evans, X. Duan, *Journal of Materials Chemistry A: Materials for Energy and Sustainability*, 1 (2013) 5840-5846.
- [27] G.Z. Hu, F. Nitze, X. Jia, T. Sharifi, H.R. Barzegar, E. Gracia-Espino, T. Wagberg, *RSC Advances*, 4 (2014) 676-682.
- [28] W. Li, Y. Huang, D. Tang, T. Zhang, Y. Wang, *Electrochimica Acta*, 174 (2015) 178-184.
- [29] J.M. Perez, B. Beden, F. Hahn, A. Aldaz, C. Lamy, *Journal of Electroanalytical Chemistry and Interfacial Electrochemistry*, 262 (1989) 251-261.
- [30] H. Hitmi, E.M. Belgsir, J.M. Leger, C. Lamy, R.O. Lezna, *Electrochimica Acta*, 39 (1994) 407-415.
- [31] N.R.d. Tacconi, R.O. Lezna, B. Beden, F. Hahn, C. Lamy, *Journal of Electroanalytical Chemistry*, 379 (1994) 329-337.
- [32] G. Tremiliosi-Filho, E.R. Gonzalez, A.J. Motheo, E.M. Belgsir, J.M. Leger, C. Lamy, *Journal of Electroanalytical Chemistry*, 444 (1998) 31-39.
- [33] D.J. Chadderton, L. Xin, J. Qi, Y. Qiu, P. Krishna, K.L. More, W. Li, *Green Chemistry*, (2014).
- [34] J. Qi, L. Xin, D.J. Chadderton, Y. Qiu, Y. Jiang, N. Benipal, C. Liang, W. Li, *Applied Catalysis B: Environmental*, 154-155 (2014) 360-368.
- [35] B. Bittins-Cattaneo, S. Wilhelm, E. Cattaneo, H.W. Buschmann, W. Vielstich, *Berichte der Bunsengesellschaft für physikalische Chemie*, 92 (1988) 1210-1218.
- [36] T. Iwasita, B. Rasch, E. Cattaneo, W. Vielstich, *Electrochimica Acta*, 34 (1989) 1073-1079.
- [37] L.W.H. Leung, S.C. Chang, M.J. Weaver, *Journal of Electroanalytical Chemistry*, 266 (1989) 317-336.

- [38] X.H. Xia, H.D. Liess, T. Iwasita, *Journal of Electroanalytical Chemistry*, 437 (1997) 233-240.
- [39] D.Z. Jeffery, G.A. Camara, *Electrochemistry Communications*, 12 (2010) 1129-1132.
- [40] M. Bellini, M. Bevilacqua, M. Innocenti, A. Lavacchi, H.A. Miller, J. Filippi, A. Marchionni, W. Oberhauser, L. Wang, F. Vizza, *Journal of the Electrochemical Society*, 161 (2014) D3032-D3043.
- [41] R.M. Van Effen, D.H. Evans, *Journal of Electroanalytical Chemistry and Interfacial Electrochemistry*, 103 (1979) 383-397.
- [42] K. Yahikozawa, K. Nishimura, M. Kumazawa, N. Tateishi, Y. Takasu, K. Yasuda, Y. Matsuda, *Electrochimica Acta*, 37 (1992) 453-455.
- [43] Z.-Z. Zhu, Z. Wang, H.-L. Li, *Journal of Power Sources*, 186 (2009) 339-343.
- [44] Y. Yan, J. Miao, Z. Yang, F.-X. Xiao, H.B. Yang, B. Liu, Y. Yang, *Chemical Society Reviews*, 44 (2015) 3295-3346.
- [45] G.K.H. Wiberg, M. Arenz, *Journal of Power Sources*, 217 (2012) 262-267.
- [46] T. Chierchie, C. Mayer, W.J. Lorenz, *Journal of Electroanalytical Chemistry and Interfacial Electrochemistry*, 135 (1982) 211-220.
- [47] G. Tremiliosi-Filho, L.H. Dall'Antonia, G. Jerkiewicz, *Journal of Electroanalytical Chemistry*, 422 (1997) 149-159.
- [48] S.M. Alia, K. Duong, T. Liu, K. Jensen, Y. Yan, *ChemSusChem*, 5 (2012) 1619-1624.
- [49] M.J. Frisch, G.W. Trucks, H.B. Schlegel, G.E. Scuseria, M.A. Robb, J.R. Cheeseman, G. Scalmani, V. Barone, B. Mennucci, G.A. Petersson, H. Nakatsuji, M. Caricato, X. Li, H.P. Hratchian, A.F. Izmaylov, J. Bloino, G. Zheng, J.L. Sonnenberg, M. Hada, M. Ehara, K. Toyota, R. Fukuda, J. Hasegawa, M. Ishida, T. Nakajima, Y. Honda, O. Kitao, H. Nakai, T. Vreven, J.A. Montgomery Jr., J.E. Peralta, F. Ogliaro, M.J. Bearpark, J. Heyd, E.N. Brothers, K.N. Kudin, V.N. Staroverov, R. Kobayashi, J. Normand, K. Raghavachari, A.P. Rendell, J.C. Burant, S.S. Iyengar, J. Tomasi, M. Cossi, N. Rega, N.J. Millam, M. Klene, J.E. Knox, J.B. Cross, V. Bakken, C. Adamo, J. Jaramillo, R. Gomperts, R.E. Stratmann, O. Yazyev, A.J. Austin, R. Cammi, C. Pomelli, J.W. Ochterski, R.L. Martin, K. Morokuma, V.G. Zakrzewski, G.A. Voth, P. Salvador, J.J. Dannenberg, S. Dapprich, A.D. Daniels, Ö. Farkas, J.B. Foresman, J.V. Ortiz, J. Cioslowski, D.J. Fox, Gaussian 09, Gaussian, Inc., Wallingford, CT, USA, 2009.
- [50] M.J.S. Dewar, W. Thiel, *Journal of the American Chemical Society*, 99 (1977) 4899-4907.
- [51] M.J.S. Dewar, E.G. Zoebisch, E.F. Healy, J.J.P. Stewart, *Journal of the American Chemical Society*, 107 (1985) 3902-3909.
- [52] J.J.P. Stewart, *Journal of Computational Chemistry*, 10 (1989) 209-220.
- [53] Z. Liu, X. Zhang, L. Hong, *Electrochemistry Communications*, 11 (2009) 925-928.
- [54] G. Hu, F. Nitze, H.R. Barzegar, T. Sharifi, A. Mikołajczuk, C.-W. Tai, A. Borodzinski, T. Wågberg, *Journal of Power Sources*, 209 (2012) 236-242.
- [55] F. Zhu, G. Ma, Z. Bai, R. Hang, B. Tang, Z. Zhang, X. Wang, *Journal of Power Sources*,

242 (2013) 610-620.

- [56] X. Zhang, P.K. Shen, *International Journal of Hydrogen Energy*, 38 (2013) 2257-2262.
- [57] S.Y. Shen, T.S. Zhao, J.B. Xu, Y.S. Li, *Journal of Power Sources*, 195 (2010) 1001-1006.
- [58] S.T. Nguyen, H.M. Law, H.T. Nguyen, N. Kristian, S. Wang, S.H. Chan, X. Wang, *Applied Catalysis B: Environmental*, 91 (2009) 507-515.
- [59] B.T.X. Lam, M. Chiku, E. Higuchi, H. Inoue, *Journal of Power Sources*, 297 (2015) 149-157.
- [60] W. Yuan, Y. Cheng, P.K. Shen, C.M. Li, S.P. Jiang, *Journal of Materials Chemistry A: Materials for Energy and Sustainability*, 3 (2015) 1961-1971.
- [61] D. Padayachee, V. Golovko, B. Ingham, A.T. Marshall, *Electrochimica Acta*, 120 (2014) 398-407.
- [62] A.K. Singh, D.M.R. Laboratory, *Advanced X-ray Techniques in Research and Industry*, IOS Press 2005.
- [63] M. Boudart, A. Aldag, J.E. Benson, N.A. Dougharty, C.G. Harkins, *Journal of Catalysis*, 6 (1966) 92-99.
- [64] S. Kozuch, J.M.L. Martin, *ACS Catalysis*, 2 (2012) 2787-2794.
- [65] H. Dohle, H. Schmitz, T. Bewer, J. Mergel, D. Stolten, *Journal of Power Sources*, 106 (2002) 313-322.
- [66] J. Liu, Z. Zhou, X. Zhao, Q. Xin, G. Sun, B. Yi, *Physical Chemistry Chemical Physics*, 6 (2004) 134-137.
- [67] C. Xie, J. Bostaph, J. Pavio, *Journal of Power Sources*, 136 (2004) 55-65.
- [68] K. Matsuoka, Y. Iriyama, T. Abe, M. Matsuoka, Z. Ogumi, *Journal of Power Sources*, 150 (2005) 27-31.
- [69] D. Kim, J. Lee, T.-H. Lim, I.-H. Oh, H.Y. Ha, *Journal of Power Sources*, 155 (2006) 203-212.
- [70] K. Scott, E. Yu, G. Vlachogiannopoulos, M. Shivare, N. Duteanu, *Journal of Power Sources*, 175 (2008) 452-457.
- [71] Z.-B. Wang, H. Rivera, X.-P. Wang, H.-X. Zhang, P.-X. Feng, E.A. Lewis, E.S. Smotkin, *Journal of Power Sources*, 177 (2008) 386-392.
- [72] Y.-C. Park, D.-H. Peck, S.-K. Kim, S. Lim, D.-H. Jung, J.-H. Jang, D.-Y. Lee, *Journal of Power Sources*, 195 (2010) 4080-4089.
- [73] J. Prabhuram, N.N. Krishnan, B. Choi, T.-H. Lim, H.Y. Ha, S.-K. Kim, *International Journal of Hydrogen Energy*, 35 (2010) 6924-6933.
- [74] G.K.S. Prakash, F.C. Krause, F.A. Viva, S.R. Narayanan, G.A. Olah, *Journal of Power Sources*, 196 (2011) 7967-7972.
- [75] S. Kang, D. Jung, J. Shin, S. Lim, S.-K. Kim, Y. Shul, D.-H. Peck, *Journal of Membrane Science*, 447 (2013) 36-42.
- [76] P. Joghee, S. Pylypenko, K. Wood, G. Bender, R. O'Hayre, *ChemSusChem*, 7 (2014)



1854-1857.

[77] F. Vigier, C. Coutanceau, A. Perrard, E.M. Belgsir, C. Lamy, *Journal of Applied Electrochemistry*, 34 (2004) 439-446.

[78] W.J. Zhou, W.Z. Li, S.Q. Song, Z.H. Zhou, L.H. Jiang, G.Q. Sun, Q. Xin, K. Poulitanitis, S. Kontou, P. Tsiakaras, *Journal of Power Sources*, 131 (2004) 217-223.

[79] W.J. Zhou, B. Zhou, W.Z. Li, Z.H. Zhou, S.Q. Song, G.Q. Sun, Q. Xin, S. Douvartzides, M. Goula, P. Tsiakaras, *Journal of Power Sources*, 126 (2004) 16-22.

[80] L. Jiang, G. Sun, S. Sun, J. Liu, S. Tang, H. Li, B. Zhou, Q. Xin, *Electrochimica Acta*, 50 (2005) 5384-5389.

[81] Z. Liu, X.Y. Ling, X. Su, J.Y. Lee, L.M. Gan, *Journal of Power Sources*, 149 (2005) 1-7.

[82] S. Song, W. Zhou, Z. Liang, R. Cai, G. Sun, Q. Xin, V. Stergiopoulos, P. Tsiakaras, *Applied Catalysis, B: Environmental*, 55 (2005) 65-72.

[83] A. Verma, S. Basu, *Journal of Power Sources*, 145 (2005) 282-285.

[84] A. Verma, A.K. Jha, S. Basu, *Journal of Power Sources*, 141 (2005) 30-34.

[85] W.J. Zhou, S.Q. Song, W.Z. Li, Z.H. Zhou, G.Q. Sun, Q. Xin, S. Douvartzides, P. Tsiakaras, *Journal of Power Sources*, 140 (2005) 50-58.

[86] S. Rousseau, C. Coutanceau, C. Lamy, J.M. Leger, *Journal of Power Sources*, 158 (2006) 18-24.

[87] F. Colmati, E. Antolini, E.R. Gonzalez, *Applied Catalysis, B: Environmental*, 73 (2007) 106-115.

[88] H. Li, G. Sun, L. Cao, L. Jiang, Q. Xin, *Electrochimica Acta*, 52 (2007) 6622-6629.

[89] J. Ribeiro, D.M. dos Anjos, K.B. Kokoh, C. Coutanceau, J.M. Léger, P. Olivi, A.R. de Andrade, G. Tremiliosi-Filho, *Electrochimica Acta*, 52 (2007) 6997-7006.

[90] P.E. Tsiakaras, *Journal of Power Sources*, 171 (2007) 107-112.

[91] J.R. Varcoe, R.C.T. Slade, E.L.H. Yee, S.D. Poynton, D.J. Driscoll, *Journal of Power Sources*, 173 (2007) 194-199.

[92] A. Verma, S. Basu, *Journal of Power Sources*, 174 (2007) 180-185.

[93] X. Xue, J. Ge, T. Tian, C. Liu, W. Xing, T. Lu, *Journal of Power Sources*, 172 (2007) 560-569.

[94] S. Basu, A. Agarwal, H. Pramanik, *Electrochemistry Communications*, 10 (2008) 1254-1257.

[95] N. Fujiwara, Z. Siroma, S.-i. Yamazaki, T. Ioroi, H. Senoh, K. Yasuda, *Journal of Power Sources*, 185 (2008) 621-626.

[96] H. Hou, G. Sun, R. He, Z. Wu, B. Sun, *Journal of Power Sources*, 182 (2008) 95-99.

[97] T. Lopes, E. Antolini, E.R. Gonzalez, *International Journal of Hydrogen Energy*, 33 (2008) 5563-5570.

[98] J. Ribeiro, D.M. dos Anjos, J.M. Leger, F. Hahn, P. Olivi, A.R. de Andrade, G. Tremiliosi-Filho, K.B. Kokoh, *Journal of Applied Electrochemistry*, 38 (2008) 653-662.

- [99] C.-C. Yang, S.-J. Chiu, K.-T. Lee, W.-C. Chien, C.-T. Lin, C.-A. Huang, *Journal of Power Sources*, 184 (2008) 44-51.
- [100] C.-C. Yang, Y.-J. Lee, S.-J. Chiu, K.-T. Lee, W.-C. Chien, C.-T. Lin, C.-A. Huang, *Journal of Applied Electrochemistry*, 38 (2008) 1329-1337.
- [101] V. Bambagioni, C. Bianchini, A. Marchionni, J. Filippi, F. Vizza, J. Teddy, P. Serp, M. Zhiani, *Journal of Power Sources*, 190 (2009) 241-251.
- [102] C. Bianchini, V. Bambagioni, J. Filippi, A. Marchionni, F. Vizza, P. Bert, A. Tampucci, *Electrochemistry Communications*, 11 (2009) 1077-1080.
- [103] A.O. Neto, R.W.R. Verjullo-Silva, M. Linardi, E.V. Spinacé, *Ionics*, 16 (2009) 85-89.
- [104] F.J.R. Varela, O. Savadogo, *Asia-Pacific Journal of Chemical Engineering*, 4 (2009) 17-24.
- [105] C. Venkateswara Rao, B. Viswanathan, *The Journal of Physical Chemistry C*, 113 (2009) 18907-18913.
- [106] M. Zhu, G. Sun, Q. Xin, *Electrochimica Acta*, 54 (2009) 1511-1518.
- [107] D. Gaurava, A. Verma, D.K. Sharma, S. Basu, *Fuel Cells (Weinheim, Germany)*, 10 (2010) 591-596.
- [108] E. Lee, A. Murthy, A. Manthiram, *Electrochimica Acta*, 56 (2010) 1611-1618.
- [109] J.B. Xu, T.S. Zhao, S.Y. Shen, Y.S. Li, *International Journal of Hydrogen Energy*, 35 (2010) 6490-6500.
- [110] L. An, T.S. Zhao, *Energy & Environmental Science*, 4 (2011) 2213-2217.
- [111] H. Hou, S. Wang, Q. Jiang, W. Jin, L. Jiang, G. Sun, *Journal of Power Sources*, 196 (2011) 3244-3248.
- [112] H. Hou, S. Wang, W. Jin, Q. Jiang, L. Sun, L. Jiang, G. Sun, *International Journal of Hydrogen Energy*, 36 (2011) 5104-5109.
- [113] Y.S. Li, T.S. Zhao, *International Journal of Hydrogen Energy*, 36 (2011) 7707-7713.
- [114] S. Shen, T.S. Zhao, J. Xu, Y. Li, *Energy & Environmental Science*, 4 (2011) 1428-1433.
- [115] M. Unlu, D. Abbott, N. Ramaswamy, X. Ren, S. Mukerjee, P.A. Kohl, *Journal of the Electrochemical Society*, 158 (2011) B1423-B1431.
- [116] J. Datta, A. Dutta, M. Biswas, *Electrochemistry Communications*, 20 (2012) 56-59.
- [117] F.L.S. Purgato, S. Pronier, P. Olivi, A.R. de Andrade, J.M. Leger, G. Tremiliosi-Filho, K.B. Kokoh, *Journal of Power Sources*, 198 (2012) 95-99.
- [118] S.C. Zignani, V. Baglio, J.J. Linares, G. Monforte, E.R. Gonzalez, A.S. Arico, *Electrochimica Acta*, 70 (2012) 255-265.
- [119] R. Chetty, K. Scott, *Journal of Applied Electrochemistry*, 37 (2007) 1077-1084.
- [120] L. Demarconnay, S. Brimaud, C. Coutanceau, J.M. Léger, *Journal of Electroanalytical Chemistry*, 601 (2007) 169-180.
- [121] V. Livshits, M. Philosoph, E. Peled, *Journal of Power Sources*, 178 (2008) 687-691.
- [122] L. Xin, Z. Zhang, J. Qi, D. Chadderton, W. Li, *Applied Catalysis, B: Environmental*, 125

(2012) 85-94.

[123] S.R. Ragsdale, C.B. Ashfield, *ECS Transactions*, 16 (2008) 1847-1854.

[124] A. Ilie, M. Simoes, S. Baranton, C. Coutanceau, S. Martemianov, *Journal of Power Sources*, 196 (2011) 4965-4971.

[125] Z. Zhang, L. Xin, J. Qi, D.J. Chadderton, W. Li, *Applied Catalysis B: Environmental*, 136-137 (2013) 29-39.

